Reconstruction of global surface ocean pCO_2 using region-specific predictors based on a stepwise FFNN regression algorithm

Guorong Zhong[1,2,3,4], Xuegang Li[1,2,3,4*], Jinming Song[1,2,3,4*], Baoxiao Qu[1,3,4], Fan Wang[1,2,3,4], Yanjun Wang[1,4], Bin Zhang[1,4], Xiaoxia Sun[1,2,3,4], Wuchang Zhang[1,3,4], Zhenyan Wang[1,3,4], Jun Ma[1,3,4], Huamao Yuan[1,2,3,4], Liqin Duan[1,2,3,4]

[1]Institute of Oceanology, Chinese Academy of Sciences, Qingdao 266071, China
[2]University of Chinese Academy of Sciences, Beijing 101407, China
[3]Pilot National Laboratory for Marine Science and Technology, Qingdao 266237, China
[4]Center for Ocean Mega-Science, Chinese Academy of Sciences, Qingdao 266071, China

Correspondence to: Xuegang Li (lixuegang@qdio.ac.cn); Jinming Song (jmsong@qdio.ac.cn)

Abstract: Various machine learning methods were attempted in the global mapping of surface ocean partial pressure of CO_2 (pCO_2) to reduce the uncertainty of global ocean CO_2 sink estimate due to undersampling of pCO_2. In previous researches the predictors of pCO_2 were usually selected empirically based on theoretic drivers of surface ocean pCO_2 and same combination of predictors were applied in all areas unless lack of coverage. However, the differences between the drivers of surface ocean pCO_2 in different regions were not considered. In this work, we combined the stepwise regression algorithm and a Feed Forward Neural Network (FFNN) to selected predictors of pCO_2 based on mean absolute error in each of the 11 biogeochemical provinces defined by Self-Organizing Map (SOM) method. Based on the predictors selected, a monthly global 1° × 1° surface ocean pCO_2 product from January 1992 to August 2019 was constructed. Validation of different combination of predictors based on the SOCAT dataset version 2020 and independent observations from time series stations was carried out. The prediction of pCO_2 based on region-specific predictors selected by the stepwise FFNN algorithm were more precise than that based on predictors from previous researches. Appling of a FFNN size improving algorithm in each province decreased the mean absolute error (MAE) of global estimate to 11.32 μatm and the root mean square error (RMSE) to 17.99 μatm. The script file of the stepwise FFNN algorithm and pCO_2 product are distributed through the Institute of Oceanology of the Chinese Academy of Sciences Marine Science Data Center (IOCAS; http://dx.doi.org/10.12157/iocas.2021.0022, Zhong et al., 2021).

1 Introduction

As a net sink for atmospheric CO_2, global oceans have been thought to have removed about one third of anthropogenic CO_2 since the beginning of the industrial revolution (Sabine et al., 2004; Friedlingstein et al., 2019). However, , due to large uncertainty in estimates of surface ocean partial pressure of CO_2 (pCO_2), the long-term average global ocean sea-air CO_2 flux during 2001-2015 estimated based on sea-air pCO_2 difference differ from -1.55 to -1.74 PgC yr^{-1}, and the maximum difference between global sea-air CO_2 flux in individual years reached nearly 0.6 PgC yr^{-1} (Rödenbeck et al., 2014; Iida et al., 2015; Landschützer et al., 2014; Denvil-Sommer et al., 2019). The magnitude and direction of the flux is largely set by the air-sea pCO_2 difference. Greater pCO_2 of surface water than that of overlying air indicating that CO_2 released from oceans to the air, and absorption of CO_2 by oceans happened when the pCO_2 of surface water was lower than that of air. The ocean in these two scenarios is known as oceanic carbon source and oceanic carbon sink respectively. Sparse and uneven observations of surface ocean pCO_2 in time and space severely limited the understanding of interannual variability of oceanic carbon sink, and researches based on different methods were carried out to break this barrier. In earlier studies, traditional unitary and multiple regression methods between surface ocean pCO_2 and its drivers was attempted in the mapping of surface ocean pCO_2, which were limited in specific regions and sometimes even in specific seasons with a relatively high root mean square error (RMSE) (Sarma et al., 2006; Takahashi et al., 2006; Shadwick et al., 2010; Chen et al., 2011; Marrec et al., 2015). Recent researches on artificial neural networks and other machine learning algorithms, such as feed-forward neural network (FFNN) method (Zeng et al., 2014; Zeng et al., 2015; Moussa et al., 2016; Denvil-Sommer et al., 2019) and self-organization mapping (SOM) method (Friedrich and Oschlies, 2009; Telszewski et al., 2009; Hales et al., 2012; Nakaoka et al., 2013), significantly reduced the bias in the interpolation based on relationships between surface ocean pCO_2 and its drivers. In addition, methods such as finding better predictors or combining SOM and other neural networks were also attempt to further decrease the pCO_2 predicting error (Hales et al., 2012; Nakaoka et al., 2013; Landschützer et al., 2014; Chen et al., 2019; Denvil-Sommer et al., 2019; Zhong et al., 2020; Wang et al., 2021). However, the selection of predictors in the surface ocean pCO_2 mapping was more empirical, focusing on the theoretical drivers of the pCO_2 and its variation. Sea surface temperature and salinity, related to the solubility of CO_2 in seawater, were considered as the most important and used in almost all related studies (Landschützer et al., 2013;

Nakaoka et al., 2013; Moussa et al., 2016; Laruelle et al., 2017; Zeng et al., 2017; Denvil-Sommer et al., 2019). Similarly, the chlorophyll-a concentration is also widely used (Nakaoka et al., 2013; Landschützer et al., 2014; Laruelle et al., 2017; Zeng et al., 2017; Denvil-Sommer et al., 2019), which is related to the phytoplankton uptake of CO_2. One more indicator, mixed layer depth, appeared frequently in related studies as a proxy related to the vertical transport of dissolved carbon (Telszewski et al., 2009; Nakaoka et al., 2013; Landschützer et al., 2014; Zeng et al., 2017; Denvil-Sommer et al., 2019). Besides, the sampling information have been also used as indicators, including latitude and longitude (Friedrich and Oschlies, 2009; Jo et al., 2012; Zeng et al., 2015; Zeng et al., 2017; Denvil-Sommer et al., 2019), and sampling time (Friedrich and Oschlies, 2009; Zeng et al., 2015). In recent researches, dry air mixing ratio of atmospheric CO_2 (xCO_2), related to the CO_2 level in air, was also used as a predictor of surface ocean pCO_2 (Landschützer et al., 2014; Denvil-Sommer et al., 2019). The sea surface height, which was considered effective in improving the spatial pattern and the accuracy of surface ocean pCO_2 mapping at the basin and regional scale, and the monthly anomalies of the most widely used parameters mentioned above were used by the Denvil-Sommer et al (2019). In the research focused on the surface ocean pCO_2 mapping of coastal areas, the bathymetry, sea ice and wind speed were also used as indicators (Laruelle et al., 2017). In each of these researches, same combination of indicators was applied in all areas of the global ocean, although the global ocean was divided into several biogeochemical provinces in some of the researches. However, the indicator that plays an important role in the surface ocean pCO_2 reconstruction at one region may be not a good predictor of surface ocean pCO_2 in other regions, due to complex and variable drivers in different regions. But no widely recognized methods for judging the importance of each predictor in the surface ocean pCO_2 mapping are available yet. Thus, we attempted to construct a stepwise FFNN algorithm to rank the importance of predictors and figure out the optimal combination in each biogeochemical province defined by SOM, for decreasing the predication errors in the surface ocean pCO_2 mapping.

2 Methodology

2.1 Data

The surface ocean fugacity of CO_2 (fCO_2) observation data from the Surface Ocean CO_2 Atlas fCO_2 dataset version 2020 (SOCATv2020) (Bakker et al., 2016) was used to construct the non-liner relationship between surface ocean pCO_2 and predictors. The conversion between fCO_2 and pCO_2 was following the formula (Körtzinger, 1999):

$$fCO_2 = pCO_2 \cdot exp\left(P \cdot \frac{B+2\delta}{RT}\right) \quad (1)$$

where fCO_2 and pCO_2 are in micro-atmospheres (µatm), P is the total atmospheric surface pressure (Pa) using the National Centers for Environmental Prediction (NCEP) monthly mean sea level pressure product (Dee et al., 2011), and T is the absolute temperature (K). R is the gas constant (8.314 J K^{-1} mol^{-1}). Parameters B (m^3 mol^{-1}) and δ (m^3 mol^{-1}) are both viral coefficients (Weiss, 1974).

In this work, total 33 indicators were used (Table S1). Where 21 indicators were chosen from previous researches of surface ocean pCO_2 reconstruction based on machine learning methods, including sea surface temperature (SST) and sea surface salinity (SSS) using the 1°×1° gridded product (Cheng et al., 2016; Cheng et al., 2017; Cheng et al., 2020) at http://www.ocean.iap.ac.cn/ and the anomalies (SST_{anom} and SSS_{anom}), chlorophyll-a concentration (CHL-a) and the anomaly (CHL-a $_{anom}$) using satellite derived monthly product in 9 km resolution (NASA Goddard Space Flight Center, Ocean Ecology Laboratory, Ocean Biology Processing Group, 2018), mixed layer depth (MLD) and sea surface height (SSH) and the anomalies (MLD_{anom} and SSH_{anom}) using the ECCO2 cube92 daily product (Menemenlis et al., 2008), dry air mixing ratio of atmospheric CO_2 (xCO_2) and the anomaly ($xCO_{2\ anom}$) from the GLOBAL VIEW marine boundary layer product (GLOBALVIEW-CO2, 2011), sea ice area fraction using the monthly product from ECMWF ERA Interim(Dee et al., 2011), 10 meters wind speed using the monthly product from ECMWF ERA Interim (Dee et al., 2011), bathymetry from ETOPO2 (Commerce et al., 2006) , year and month (represented by 1-12), the total number of months since January 1992 (N_{mon}), the sine of latitude and the sine and cosine of longitude (sLat, sLon and cLon). In addition, 12 parameters which were only used in similar previous research focused on other parameters (Broullón et al., 2019; Broullón et al., 2020), or were possibly related to the driver of surface ocean pCO_2 and its variability, were selected to be tested. These parameters included nitrate, phosphate, silicate and dissolved oxygen (DO) using the monthly climatology product from WOA18 (Garcia et al., 2019a, b), sea level pressure (SLP) and surface pressure from the ECMWF ERA Interim (Dee et al., 2011), W velocity of ocean currents (W_{vel}) at 5, 65, 105 and 195 m depth using the ECCO2 cube92 3-day product (Menemenlis et al., 2008), the Oceanic Nino Index (ONI) (Huang et al., 2017), the Southern Hemisphere Annular Mode Index (SAM) (Marshall, G. J., 2003). Most of these products were retrieved at 1° × 1° resolution. Some products retrieved at higher resolution were downscaled to 1° × 1° resolution.

2.2 Biogeochemical provinces defined by the Self-Organizing Map

For applying different combination of indicators in regions based on the differences in the dominated drivers of pCO_2 and its variability, the global ocean was divided into a set of biogeochemical provinces using a Self-Organizing Map (SOM) method. The monthly climatology of temperature, salinity, mixed layer depth, sea surface height, nitrate, phosphate, silicate, and dissolved oxygen and pCO_2 climatology from Landschützer et al, 2020 were put into a 3-by-4 size SOM networks to generate 12 biogeochemical provinces, where the monthly climatology data in all 12 months were put into one SOM network to generate one discrete set of biogeochemical provinces. Provinces with connected pixels less than 10 and provinces with SOCAT observation less than 1000 were define as discrete small "island" provinces, and then merged with nearest provinces. The provinces covering areas separated by land were further divided artificially. For example, the province covering north subtropical Pacific and the province covering north subtropical Atlantic were set as one province in the original output of SOM, but were mainly separated by The North American continent. So, we divided the province into two new provinces. The final version includes total 11 biogeochemical provinces. In this study the coastal area was not involved and the boundary was defined as 200m depth. In addition, the pCO_2 mapping based on SOM defined provinces tend to be less smooth near the border of different biogeochemical provinces, with obvious border line appearing. However, applying of different predictors may make this problem worse. To obtain a smoother distribution, we defined that the area within 5 1x1 grids of province boundaries as a 'boundary area'. Samples in the boundary area will be used as training samples in all adjacent provinces (Fig. S1). But this definition does not change the actual spatial coverage of each province, only brings more training samples near the province boundary.

2.3 Stepwise FFNN algorithm

For finding better combination of pCO_2 predictors, a stepwise Feed-forward neural networks (FFNN) algorithm was constructed. The FFNN is composed of four main parts, which are namely input, hidden, summation and output layer (Fig. 1). The input layer is designed to pass the inputs to the hidden layer and the number of neurons is equal to the dimensions of the input matrix p. The hidden layer includes 25 neurons in the FFNN model, with the tan-sigmoid function as the transfer function. The input p is multiplied by a matrix of weights (w_1 in Fig. 1) and the inner product between the result and a bias matrix (b_1 in Fig. 1) is calculated as the input of the transfer function in the first hidden layer. In the summation layer, the transfer function f_2 is a pure linear function. The output of the hidden layer is multiplied by another matrix of weights and summed. All bias and weights matrixes were randomly assigned in the beginning of FFNN training. Here we set one constant random number stream in the MATLAB, thus the way that the bias and weights matrixes randomly assigned were steady, avoiding the appearance of inconsistent results when algorithm repeats.

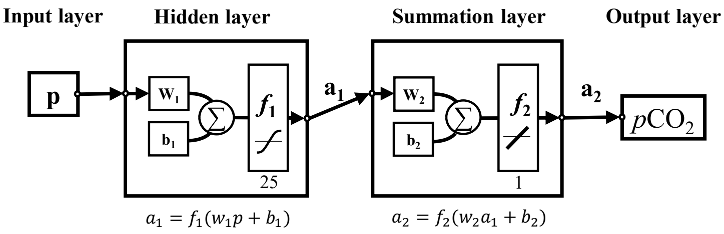

Figure 1. The structure of feed-forward neural network. **p**: input matrix; **w**: weighted matrix; **b**: bias matrix; ∑: sum; $\boldsymbol{f_1}$: tan-sigmoid transfer function; $\boldsymbol{f_2}$: pure linear function; **a**: output matrix.

In the stepwise part, predictors of $p\mathrm{CO_2}$ are going to be added and removed one by one, and which predictors will be finally used in the $p\mathrm{CO_2}$ predicting is determined according to the real-time change of predicating error. The mean absolute error (MAE) difference that before and after adding or removing one indicator in the input of FFNN calculated using a K-fold cross validation method was used to estimate the performance of each indicator in the FFNN predicating. Although the root mean square error (RMSE) was widely used for the validation of machine learning methods. Compared to the MAE, the RMSE was more sensitive to a few extreme samples, which were generally deviated far from the FFNN predicting values, resulting in a huge discrepancy between the FFNN outputs and $p\mathrm{CO_2}$ observations sometimes up to hundreds of μatm. A higher weight may be put on these few extreme samples than other samples in the predictor selection if the performance of each indicator was estimated by RMSE in the stepwise FFNN algorithm. To avoid the higher weight on these few extreme samples, the MAE was used instead for internal performance loss function in the stepwise FFNN algorithm. The basic principle of the stepwise FFNN algorithm was adding each indicator from a set of indicators into the inputs of FFNN and removing each redundant indicator from the inputs successively to reduce the MAE between the FFNN outputs and SOCAT $p\mathrm{CO_2}$ values in the fastest way, until no decrease in the MAE appearing (Fig. 2), where the indicator having no contribution to reduce the prediction error was considered as redundant.

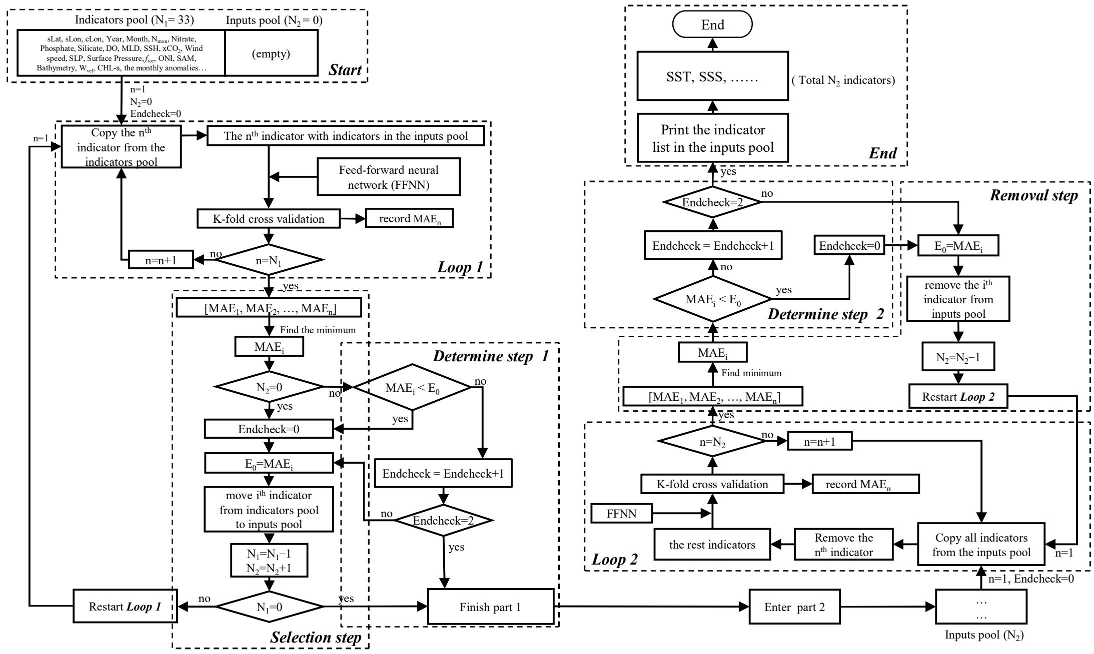

Figure 2. The procedure of stepwise FFNN algorithm. The flow-chart is following an order of "left top – left bottom – right bottom – right top". The meaning of Indicators pool: store all indicators waiting to be tested; Inputs pool: store indicators that was temporally considered as good predictors; *Loop 1* and *Loop 2*: calculate the MAE when each indicator was added as predictors or removed; Selection step: add good predictors to the Inputs pool; *Removal step*: remove predictors from the Inputs pool if removing lead to MAE decrease; *Determine step*: check if the process reach end condition. N_1 and N_2: number of indicators in the Indicators pool and Inputs pool respectively; E_0: lowest MAE in the last iteration of *Loop 1* or *Loop 2*; Endcheck: the number of iterations that E_0 continuously increased.

In the beginning of the stepwise FFNN algorithm, all available indicators were put into a matrix, referred to as indicators pool (*Start* in Fig. 2), where each of rows represents one indicator and each of columns represents one SOCAT sample. In this work we collected 33 parameters for test, that is, the indicators pool matrix has 33 rows. Meanwhile a matrix, referred to as inputs pool (*Start* in Fig. 2), was set up to store indicators with good performance, where good performance means that adding these indicators as predictors can significantly decrease the MAE between SOCAT $p\mathrm{CO_2}$ measurements and FFNN $p\mathrm{CO_2}$ predictions. Then a loop of K-fold validation test run out to calculate the MAE that predicting $p\mathrm{CO_2}$ by each one indicator in the indicators pool in the first step (*Loop 1* in the Fig. 2). Thus total 33 MAE values were obtained and the minimum was recorded as E_0. The indicator that corresponds to the minimum of all MAE values was moved from the indicators pool to the inputs pool (*Selection step* in the Fig. 2). After that the loop 1 restarted, i.e., the second step started with one indicator removed to the inputs pool and the rest 32 indicators waiting to be tested. Then 32 MAE values of predicting pCO_2 by each one of the rest indicators in the indicators pool with the addition of all indicators in the inputs pool were calculated out. If the MAE in the lowest situation, represented by the MAE_i, decreased compared to the E_0, the i^{th} indicator was considered as a good indicator and was moved from the indicators pool to the inputs pool as well. Then the value of E_0 was replaced by the MAE_i (*Selection step* in the Fig. 2). The part 1, including *loop 1*, *Selection step* and *Determine step* in the Fig. 2, was repeated that the good indicators were selected out in one-by-one step and moved to the inputs pool in the way that the E_0 decreases in the fastest way, until no indicator was left in the indicators pool or no decrease can be found no matter which indicator was added in the next two steps (*Determine step 1* in the Fig. 2). At this time the part 1 of stepwise FFNN algorithm finished, and all indicators left in the indicators pool were considered redundant. The loop K-fold validation in the second part run out in a opposite way that the MAE was calculated with the indicators were removed from the inputs pool one by one in the way that the E_0 decreases the fastest (*Loop 2* in Fig. 2). The second part was aimed to remove the indicator that can be represented by other indicators in the inputs pool (*Removal step* in the Fig. 2), and finished in the similar condition that no significant decrease can be found no matter which indicator was removed in the next two steps (*Determine step 2* in the Fig. 2).

2.4 pCO_2 product

Dataset of parameters except CHL-a start since 1992 or earlier, while CHL-a data ranges from August 2002 to present. In each one of the provinces, the stepwise FFNN algorithm was run out once first based on all samples covered by CHL-a data, then the algorithm was run out secondly based on samples and all indicators except CHL-a and CHL-a_{anom} in the year that CHL-a gridded data was not available. The pCO_2 mapping in the year that CHL-a gridded data was not available was carried out based on the predictors selected in the second run. Then the final product was built based on two FFNNs, one trained for the period from August 2002 to August 2019 using one predictor set including CHL-a or CHL-a_{anom}, and the second one for the period from January 1992 to July 2002 using the second predictor set without CHL-a and CHL-a_{anom}. Although the performance may improve with the number of neurons increasing, the influence of number of neurons on the performance of FFNN pCO_2 prediction remains unclear. To further decrease the predicating error between FFNN outputs and SOCAT measurements, the number of neurons was improved by an error test in each province. The number of neurons increased from 5 to 300 and the corresponding MAE values of each size were record, and then the number of neurons with lowest MAE was applied. This test avoided the appearance of insufficient learning capacity for complex nonlinear relationship due to too few neurons and overfitting problem due to too many neurons. Finally, based on the indicators selected by the stepwise FFNN algorithm and improved FFNN size, a monthly global 1°×1° surface ocean pCO_2 product from January1992 to August 2019 was constructed.

2.5 Validation

To better estimate the predicating error of FFNN, the MAE and additionally the RMSE which was widely used in previous researches, were calculated using a K-fold cross validation method. To avoid overfitting caused by a lack of independence between the training samples and testing samples, the SOCAT samples were put in chronological order and then divided into group of years (Table 1) (Gregor et al., 2019). In this paper, the value of K was set as 4. Thus, among every 4 neighboring years, three group samples were used for training FFNN model and the rest one was used for testing. Total 4 iterations were carried out, where testing year changed in each iteration. After 4 iterations finished, all samples have been used for testing only once, and the MAE and RMSE between FFNN output and the testing samples was calculated. The performance of the predictor selection algorithm was estimated by comparing the MAE and RMSE result of the FFNN based on stepwise selected indicators with the result based on indicators used in previous researches in each biogeochemical province (Table 2). All validation groups were applied with same FFNN and same samples from SOCAT, with the only differences in predictors. Same K-fold validation procedure was applied for three validation groups based on different pCO_2 predictors. Thus, three results were generated to estimate whether the stepwise FFNN algorithm can effectively find better combination of pCO_2 predictors. Finally the pCO_2 data generated in all validation groups were further compared with the completely independent observations from the Hawaii Ocean Time-series (HOT, 22° 45'N, 158° 00'W, since October 1988) (Dore et al., 2009), Bermuda Atlantic Time-series Study (BATS, 31°50'N, 64°10'W, since October 1988) (Bates, 2007) and The European Station for Time Series in the Ocean Canary Islands (ESTOC, 29°10′N, 15°30′W, from 1995 to 2009) (González-Dávila and Santana-Casiano, 2009) time series station. These observations were not included in the SOCAT dataset.

Table 1. The procedure of K-fold validation.

	FFNN training	**FFNN testing**															
1st iteration	**1992**	1993	1994	1995	**1996**	1997	1998	1999	…	**2012**	2013	2014	2015	**2016**	2017	2018	2019
2nd	1992	**1993**	1994	1995	1996	**1997**	1998	1999	…	2012	**2013**	2014	2015	2016	**2017**	2018	2019
3rd	1992	1993	**1994**	1995	1996	1997	**1998**	1999	…	2012	2013	**2014**	2015	2016	2017	**2018**	2019
4th iteration	1992	1993	1994	**1995**	1996	1997	1998	**1999**	…	2012	2013	2014	**2015**	2016	2017	2018	**2019**

(The K value was set as 4, so iterations repeated four times until all samples have been set as testing samples once. In each iteration, samples in 7 years were set as testing samples (green cells) and in the rest 21 years as training samples (white cells) to increase the independency.)

Table 2. Validation group using different predictors

Validation group	Predictor
FFNN1	Indicators selected by stepwise FFNN algorithm
FFNN2	SST, SSS, $\log_{10}$(MLD), CHL-a, xCO_2, SST_{anom}, SSS_{anom}, $xCO_{2\ anom}$, CHL-a $_{anom}$, $\log_{10}$(MLD) $_{anom}$ (Landschützer et al., 2014)
FFNN3	SST, SSS, SSH, MLD, xCO_2, CHL-a, SSS_{anom}, SST_{anom}, SSH_{anom}, CHL-a $_{anom}$, MLD_{anom}, $xCO_{2\ anom}$, sLat, sLon, cLon (Denvil-Sommer et al., 2019)

(The FFNN performance of three groups with different predictors of pCO_2 were compared, to test the result of stepwise FFNN algorithm. Predictors in the group FFNN1 were selected using stepwise FFNN algorithm, and predictors in the group FFNN2 were selected from Landschützer et al. (2014), and in the group FFNN3 from Denvil-Sommer et al. (2019).)

3 Results and discussion

3.1 Biogeochemical provinces and corresponding predictors of pCO_2

11 biogeochemical provinces generated from the SOM method after the separated small 'island' was removed and the province separated by lands was divided manually (Fig. 3). The results of the stepwise FFNN algorithm in each province were shown in the Table 3. The indicators were listed in the order that the stepwise FFNN algorithm printed recommended predictors out. The indicator printed earlier was relatively more recommended and played an important role in the prediction of pCO_2 based on FFNN. Applying of these indicators as the predictors of surface ocean pCO_2 effectively decreased the predicating error between the FFNN outputs and pCO_2 values from validation samples, thus it is reasonable to consider that these indicators were highly

related to the drivers of pCO_2 and its variability. Indicators representing sampling position were also listed as recommended predictors in some provinces, including latitude, longitude and sampling time, suggesting that relatively steady spatial or temporal variability pattern of surface ocean pCO_2 existed in these biogeochemical provinces. For example, month was considered as a recommended predictor in most provinces. Especially in the province P4 subpolar Atlantic and P5 north subtropical Atlantic, the parameter month was relatively more recommended. While pCO_2 in these areas regularly peaked and bottomed out in summer and winter (Takahashi et al., 2009; Landschützer et al., 2016; Landschützer et al., 2020). Similarly, latitude and the sine and cosine of longitude were listed as recommended predictors of pCO_2 in most provinces, suggesting an obvious spatial distribution pattern of pCO_2, which was not learned sufficiently by the FFNN model from existing indicators and the indicators related to spatial position were applied as supplementary.

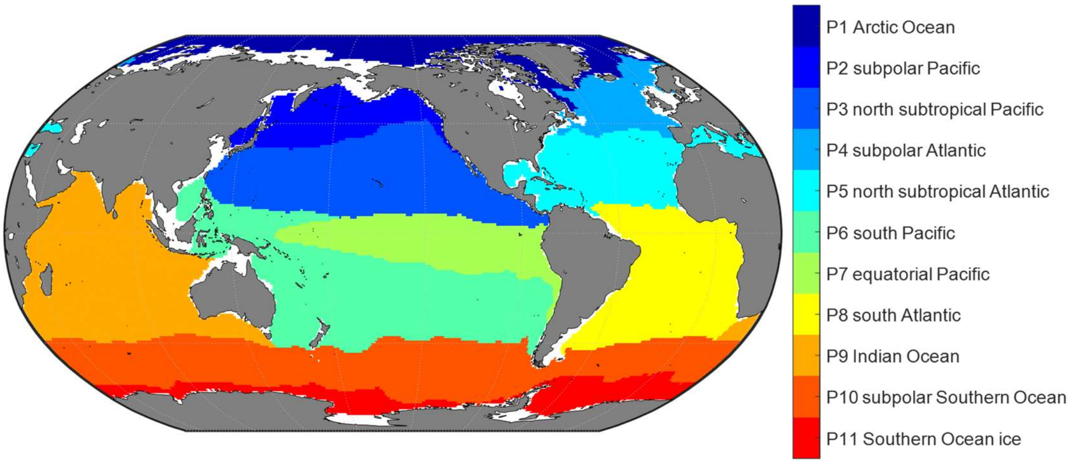

Figure 3. The map of biogeochemical provinces

As basic parameters highly related to the ocean environment, the temperature and salinity was considered as parts of the most important predictors of surface ocean pCO_2, and was applied in the pCO_2 prediction in almost all previous relating researches based on various method (Jo et al., 2012; Signorini et al., 2013; Landschützer et al., 2014; Marrec et al., 2015; Chen et al., 2016; Moussa et al., 2016; Chen et al., 2017; Laruelle et al., 2017; Zeng et al., 2017; Chen et al., 2019; Denvil-Sommer et al., 2019). The results of stepwise FFNN algorithm also supported this. Temperature was listed as a recommended predictor in all biogeochemical provinces, suggesting that temperature was the one of the most important drivers of pCO_2 and its variability in these provinces. Similarly, the result of stepwise FFNN algorithm provides evidence for the importance of salinity in the predication of pCO_2, which was also listed as a predictor in most provinces. The dry air mixing ratio of atmospheric CO_2 (xCO_2) and the monthly anomaly of xCO_2 were also recommended predictors in most of the biogeochemical provinces, suggesting that the exchange of CO_2 across the sea-air interface was also an important driver of surface ocean $p$$CO_2$. As a widely used predictor in the $p$$CO_2$ prediction, the chlorophyll-a concentration (CHL-a) played an important role in fitting the influence of biological activities on $p$$CO_2$ in previous researches (Landschützer et al., 2014; Zeng et al., 2017; Laruelle et al., 2017; Denvil-Sommer et al., 2019). Especially in the province P10 subpolar Southern Ocean and P11Southern Ocean ice, the CHL-a was listed as the most recommended predictor in the result of stepwise FFNN algorithm. While in some other provinces (P1 Arctic Ocean and P5 north subtropical Atlantic), the CHL-a were considered redundant that no effective decrease of MAE between FFNN outputs and $p$$CO_2$ measurements appeared when CHL-a data was used. Similar with the period that CHL-a was not available (represented by the subscript ‘b’), the phosphate, nitrate, silicate or dissolved oxygen were recommended instead. In the province P1 Arctic Ocean, the silicate concentration and temperature were considered as the most crucial predictor of $p$$CO_2$.

Table 3. Predictors in each biogeochemical province

Province	Predictors on the order selected by the stepwise FFNN algorithm
P1 Arctic Ocean	Silicate, SST, Wind speed, SSS, log_{10}(MLD), SSS_{anom}, sLat, month, W_{vel}(65m), log_{10}(MLD)$_{anom}$, xCO_2, cLon, Bathymetry, SSH
P2 subpolar Pacific $_{a}^{*}$	Nitrate, CHL-a, SSS, xCO_2, cLon, SST, log_{10}(MLD), sLon, sLat, month
P2 subpolar Pacific $_{b}^{*}$	Nitrate, xCO_{2anom}, sLon, SST, sLat, log_{10}(MLD), cLon, SSS, SSH_{anom}, DO, W_{vel}(195m), Bathymetry, Silicate
P3 north subtropical Pacific $_{a}$	log_{10}(MLD), N_{mon}, SSH, SST, sLon, sLat, SSS, Bathymetry, month, log_{10}(MLD)$_{anom}$, cLon, Surface pressure, W_{vel}(105m), CHL-a, DO, SSH_{anom}, $xCO_{2\ anom}$
P3 north subtropical Pacific $_{b}$	log_{10}(MLD), xCO_2, sLat, sLon, SST, Surface pressure, cLon, SSS, W_{vel}(5m), N_{mon}, log_{10}(MLD)$_{anom}$, month, Phosphate, $xCO_{2\ anom}$, W_{vel}(105m)
P4 subpolar Atlantic $_{a}$	month, sLat, cLon, SST, Year, CHL-a, DO, SSS_{anom}, W_{vel}(195m), SSH, log_{10}(MLD), Bathymetry, SSS
P4 subpolar Atlantic $_{b}$	month, xCO_2, DO, Wind speed, log_{10}(MLD), W_{vel}(195m), sLon, Bathymetry, W_{vel}(5m), SST, Phosphate, Year, N_{mon}
P5 north subtropical Atlantic	month, Year, SST, sLon, sLat, SSS, SST_{anom}, SSH, Bathymetry, W_{vel}(5m), cLon, W_{vel}(65m), log_{10}(MLD)$_{anom}$
P6 south Pacific $_{a}$	SST, sLon, $xCO_{2\ anom}$, sLat, SSS, month, Phosphate, CHL-a, CHL-a$_{anom}$,

	W_{vel}(65m), log_{10}(MLD), $log_{10}(MLD)_{anom}$, Nitrate, Bathymetry
P6 south Pacific $_b$	xCO_2, sLat, SSS, SST, Phosphate, SLP, $xCO_{2\,anom}$, sLon, cLon, W_{vel}(105m), W_{vel}(65m), DO, Bathymetry, SSH, SAM
$P7_a$ equatorial Pacific	Nitrate, xCO_2, sLat, SSS, SST, cLon, $xCO_{2\,anom}$, log_{10}(MLD), sLon, CHL-a, Phosphate, W_{vel}(5m), W_{vel}(105m), W_{vel}(195m)
$P7_b$ equatorial Pacific	SST, SSS, Year, sLat, month, cLon, SSH, Bathymetry, W_{vel}(65m), xCO_2
P8 south Atlantic $_a$	sLat, $xCO_{2\,anom}$, SSS, log_{10}(MLD), CHL-a, SSH_{anom}, W_{vel}(195m), cLon, SST, W_{vel}(65m), Bathymetry, Nitrate
P8 south Atlantic $_b$	SST, xCO_2, cLon, sLat, SSS, Silicate, SSH, log_{10}(MLD), sLon
P9 Indian Ocean $_a$	SST, cLon, sLat, Nitrate, W_{vel}(65m), log_{10}(MLD), SLP, CHL-a, Year, $log_{10}(MLD)_{anom}$, SSH_{anom}
P9 Indian Ocean $_b$	SLP, month, sLon, $xCO_{2\,anom}$, SST, Silicate, W_{vel}(65m)
P10 subpolar Southern Ocean $_a$	CHL-a, log_{10}(MLD), N_{mon}, SSS, SST, Bathymetry, SSH_{anom}, W_{vel}(5m), CHL-a $_{anom}$, xCO_2
P10 subpolar Southern Ocean $_b$	Wind speed, $xCO_{2\,anom}$, SSS, Phosphate, log_{10}(MLD), W_{vel}(65m), Bathymetry, SST, month
P11 Southern Ocean ice $_a$	CHL-a, sLon, Bathymetry, SSS, SSH, SST, Nitrate, cLon, sLat
P11 Southern Ocean ice $_b$	month, DO, SST, SSH, sLat, Nitrate, sLon, SSS, W_{vel}(195m), Silicate, SSHanom

*: Due to insufficient coverage of CHL-a data in the polar areas and during the period before 2002. In the province that CHL-a or CHL-a $_{anom}$ were selected as predictors, the pCO$_2$ data was divided into two periods. The period that CHL-a data available was represented by the subscript 'a', such as $P2_a$, including global grids from 2002 to 2019 except polar grids in winter. The period that CHL-a data not available was represented by the subscript 'b', such as $P2_b$, including global grids from 1992 to 2001 and additionally some polar grids in winter from 1992 to 2019.

3.2 *p*CO$_2$ product

Based on the predictors given by the stepwise FFNN algorithm in each biogeochemical province, a FFNN size (representing the number of neurons in the hidden layer) improving validation was applied to further decrease the predication error. The MAE values based on same samples and FFNN model with different number of neurons were calculated, then the number of neurons corresponding to the lowest MAE were applied (Fig. 4a). The MAE in most provinces tend to decrease first and then increase when the number of neurons in the hidden layer of FFNN model increased from 5 to 300. Based on the variation of MAE with the number of neurons in the FFNN hidden layer, the optimal FFNN size in each province was considered as the number of neurons when the MAE was lowest. The result and corresponding MAE were shown in

Fig. 4b. The MAE and RMSE of global estimates between predicted pCO_2 and measurements from SOCAT v2020 further decreased to 11.32 and 17.99 μatm respectively after applying optimal FFNN size in each province.

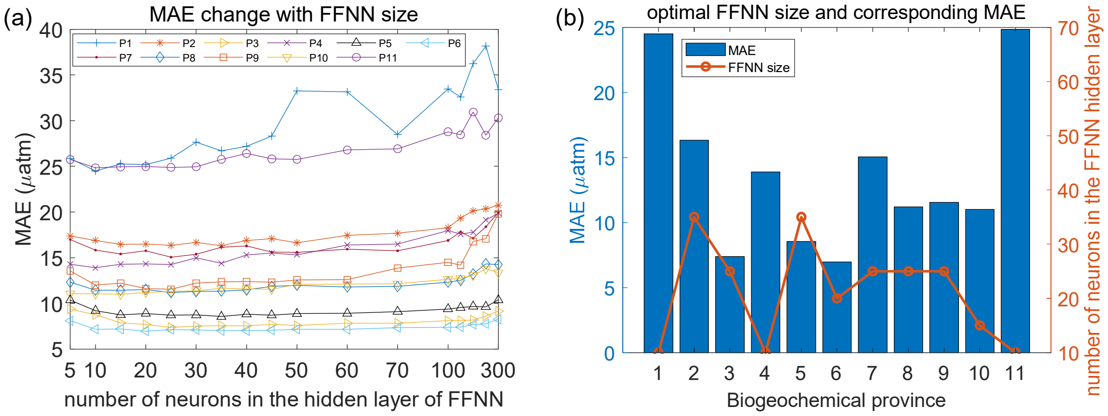

Figure 4. MAE of different FFNN size in each biogeochemical province. a): MAE between predicted pCO_2 and SOCAT observations were calculated using same samples and FFNN with different number of neurons. b): the optimal FFNN size was referring to the number of neurons when MAE is lowest.

Then the RMSE and mean residuals in each grid were calculated based on the K-fold cross validation method. In most grids, the RMSE was lower than 10 μatm and the mean residuals was close to zero (Fig. 5). However, the prediction error in the north subpolar Pacific, the east equatorial Pacific and the Southern Ocean near the Antarctic continent was obviously higher than other areas. Also, distribution of mean residuals suggested that surface ocean pCO_2 in the Indian Ocean tend to be overestimated by the FFNN models. While in other regions the distribution of mean residuals was more discrete and no obvious pattern was found.

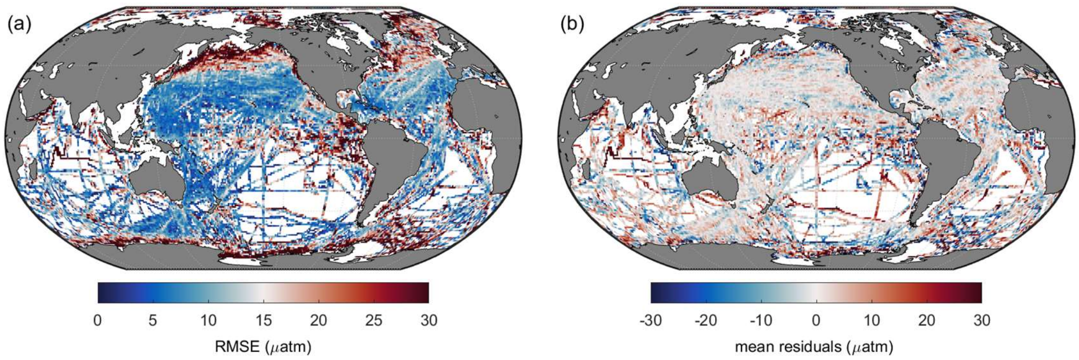

Figure 5. Global maps of (a) RMSE and (b) mean residuals between predicted pCO_2 and SOCAT observations

3.3 Validation of the stepwise FFNN algorithm based on SOCAT samples

Validation based on the K-fold cross validation method suggested that most FFNN outputs were quite close to the pCO_2 values from SOCAT v2020 samples (Fig. 6). Comparing the results based on different combination of predictors, the results of FFNN1 (based on stepwise FFNN algorithm，this paper) and FFNN3 (based on 15 predictors from Denvil-Sommer, et al. 2019) were more precise than that of FFNN2 (based on 10 predictors from Landschützer, et al. 2014). Where the plots in the result of FFNN1 was most concentrated along the y=x line, suggesting extremely close FFNN outputs with the measured pCO_2 values from SOCAT, with the RMSE of 17.99 μatm in the global open oceans. The RMSE of FFNN1 was lower than that of FFNN2 (22.95 μatm) and FFNN3 (19.17 μatm).

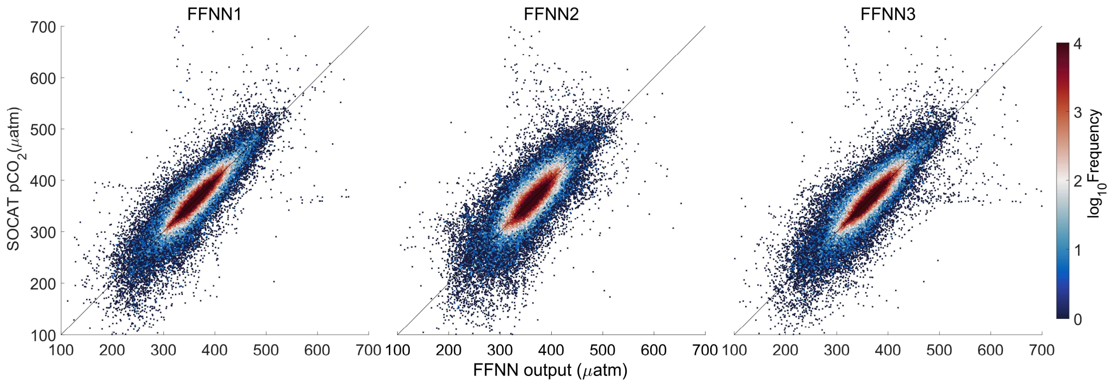

Figure 6. Comparing of FFNN predicted pCO_2 with SOCAT pCO_2. FFNN1 was based on predictors selected by the stepwise-FFNN algorithm. FFNN2 and FFNN3 were based on predictors from Landschützer et al., 2014 and Denvil-Sommer et al., 2019 respectively.

For specific comparison of accuracy in each province, the MAE of FFNN1 was lower in most provinces (Table. 4), except the relatively close results between the FFNN1 and FFNN3 in parts of provinces. Where the MAE of FFNN1 in the province P9 Indian Ocean was significantly lower than that of the other validation groups, suggesting a better combination of predictors highly related to the drivers of surface ocean pCO_2 and its variability in the Indian Ocean. Compared with predictors of FFNN2 and FFNN3, the predictors of FFNN1 added surface pressure and W velocity of ocean currents, and abandoned the monthly anomalies of other indicators in the province P9 Indian Ocean. The low relevance between pCO_2 and part of the monthly anomalies, such as SSS_{anom} and SST_{anom}, may be responsible for significant lower MAE of FFNN1. Adding redundant indicators may cause misleading in the learning of FFNN model on the contrary. The MAE and RMSE difference between FFNN1 and FFNN3 in some provinces were relatively small. The reason for higher MAE and RMSE showed by the FFNN2 may be the application of latitudes and longitudes as predictors in both the FFNN1 and FFNN3 but not in the FFNN2. In the province P10 subpolar

Southern Ocean, latitudes and longitudes were considered not good predictors by the stepwise FFNN algorithm and the results of three validation groups were extremely close.

Table 4. Performance of the pCO_2 prediction based on different predictors

Province	FFNN size	MAE (μatm)			RMSE (μatm)		
		FFNN1	FFNN2	FFNN3	FFNN1	FFNN2	FFNN3
P1 Arctic Ocean (9856)	10	**24.50**	32.32	26.87	**32.27**	43.68	35.08
P2 subpolar Pacific (30516)	35	**16.32**	20.63	16.67	**24.32**	29.87	25.03
P3 north subtropical Pacific (56367)	25	**7.39**	12.16	7.95	**11.33**	17.75	11.88
P4 subpolar Atlantic (29595)	10	**13.89**	16.91	14.73	**21.06**	24.29	22.27
P5 north subtropical Atlantic (45358)	35	**8.55**	12.28	9.00	**12.80**	17.86	13.72
P6 south Pacific (31803)	20	**6.96**	9.94	7.24	**9.86**	14.64	11.00
P7 equatorial Pacific (11233)	25	**15.05**	19.55	15.49	**20.98**	27.61	21.10
P8 south Pacific (10259)	25	**11.19**	15.07	12.43	**17.10**	20.87	17.66
P9 Indian Ocean (7440)	25	**11.54**	13.78	15.49	**17.15**	22.89	28.29
P10 subpolar Southern Ocean (21206)	15	**11.00**	11.76	12.14	**16.61**	17.22	17.66
P11 Southern Ocean ice (10683)	10	**24.84**	29.26	25.74	**34.73**	40.42	35.22
Global (264316)		**11.32**	15.08	12.06	**17.99**	22.95	19.17

(FFNN1 was based on predictors selected by the stepwise-FFNN algorithm. FFNN2 and FFNN3 were based on predictors from Landschützer et al., 2014 and Denvil-Sommer et al., 2019 respectively.)

3.4 Validation based on independent observations

The FFNN outputs based on different combination of predictors were compared with independent observations from the Ocean Time-series (HOT) (Dore et al., 2009), Bermuda Atlantic Time-series Study (BATS) (Bates, 2007) and The European Station for Time Series in the Ocean Canary Islands (ESTOC) (González-Dávila and Santana-Casiano, 2009) (Fig. 7). Compared with the independent observations from the HOT station, the three validation groups both show close results, which were also similar with each other in the seasonal and interannual variability of pCO_2. From 1992 to 2019, the RMSE between FFNN1 outputs and HOT observations was only 9.29 μatm, lower than the 10.85 μatm of FFNN2 and the 10.70 μatm of FFNN3. The monthly mean pCO_2 of FFNN2 during winter was lower than the HOT observations and pCO_2 values of other validation groups, while the FFNN1 and FFNN3 outputs were closer to the HOT observations. MAE between predicted pCO_2 and HOT observations were also lower in the validation group FFNN1, which was only 7.17 μatm, compared to the 8.61 μatm of FFNN2 and the 8.44 μatm of FFNN3. Higher bias generated in the winter bottom and summer peak, which was showed more obviously in the monthly average of pCO_2 (Fig. 7b). Compared with other validation groups, the result of FFNN1 was closer to the monthly average values of the HOT observations. Same conclusion can be obtained in the ESTOC and BATS station located in the province P5 north subtropical Atlantic. The RMSE between FFNN1 outputs and independent observations were 13.03 μatm in the BATS station and 11.35 μatm in the ESTOC station, lower than that of other validation groups. The RMSE between FFNN2 outputs and independent observations was 16.15 μatm in the BATS station and 14.51 μatm in the ESTOC station. For the group FFNN3, the RMSE was 13.09 μatm in the BATS station and 13.01 μatm in the ESTOC station. All results were extremely close to the independent observations, but the RMSE and MAE of FFNN1 were lower. Similar with the situation in the HOT station, the FFNN1 was most close and the FFNN3 second. Based on the better performance of FFNN1, in which the predictors selected by stepwise FFNN algorithm were used, we may conclude that the stepwise FFNN algorithm can effectively find better combination of predictors to fit the diver of surface ocean pCO_2 and obtained lower error.

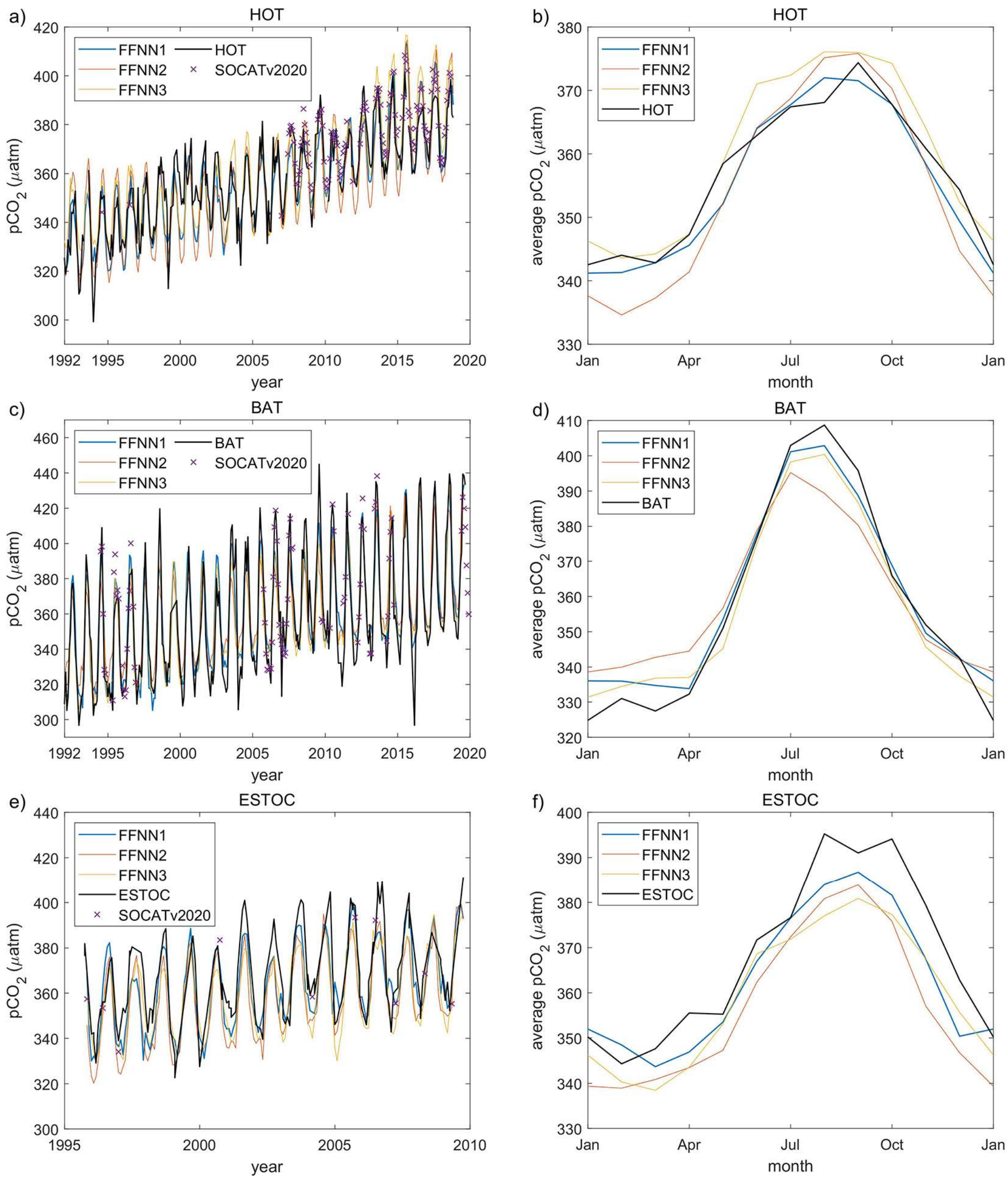

Figure 7. Validation based on independent observation from time series stations. a) and b): the Hawaii Ocean Time-series (HOT) (Dore et al., 2009); c) and d): the Bermuda Atlantic Time-series Study (BATS) (Bates, 2007); e) and f): the European Station for Time Series in the Ocean Canary Islands (ESTOC) (González-Dávila and Santana-Casiano, 2009) time series station. FFNN1 was based on predictors selected by the stepwise-FFNN algorithm. FFNN2 and FFNN3 were based on predictors from Landschützer et al., 2014 and Denvil-Sommer et al., 2019 respectively. SOCATv2020 represents the monthly mean pCO$_2$ of SOCAT observations in the corresponding grids of each time series station.

3.5 Climatological spatial distribution

The climatological average distribution of pCO$_2$ suggested a significant spatial variability (Fig. 8), which is consistent with the average distribution of SOCAT observations. In the Pacific Ocean, the high pCO_2 areas showed by the stepwise-FFNN product (Fig. 8b), including the equatorial areas, east temperate areas and north subpolar areas, were highly consistent with the SOCAT datasets (Fig. 8a). Similarly, the distribution of pCO_2 in the Atlantic Ocean was also close. However, the stepwise-FFNN product suggested lower pCO_2 average values in the Arctic and higher values in the Southern Ocean near the Antarctic continent. Compared with previous climatology product (Landschützer et al., 2020), the stepwise FFNN product have similar spatial patterns with high pCO_2 in the eastern equatorial Pacific and equatorial Atlantic: inconsistent spatial distribution also existed in the Arctic and parts of the Southern Ocean near the Antarctic continent. The differences between stepwise-FFNN product and previous climatology product may be caused by differences in methods or SOCAT dataset versions used. While lower average values of the SOCAT dataset in the Southern Ocean may be caused by the undersampling in winter. The global spatial distribution pattern of the stepwise FFNN pCO_2 product was basically well consistent with previous climatology product and SOCAT dataset, suggesting that pCO_2 predicting based on regional different predictors selected by the stepwise FFNN algorithm was better than that based on the globally same predictors.

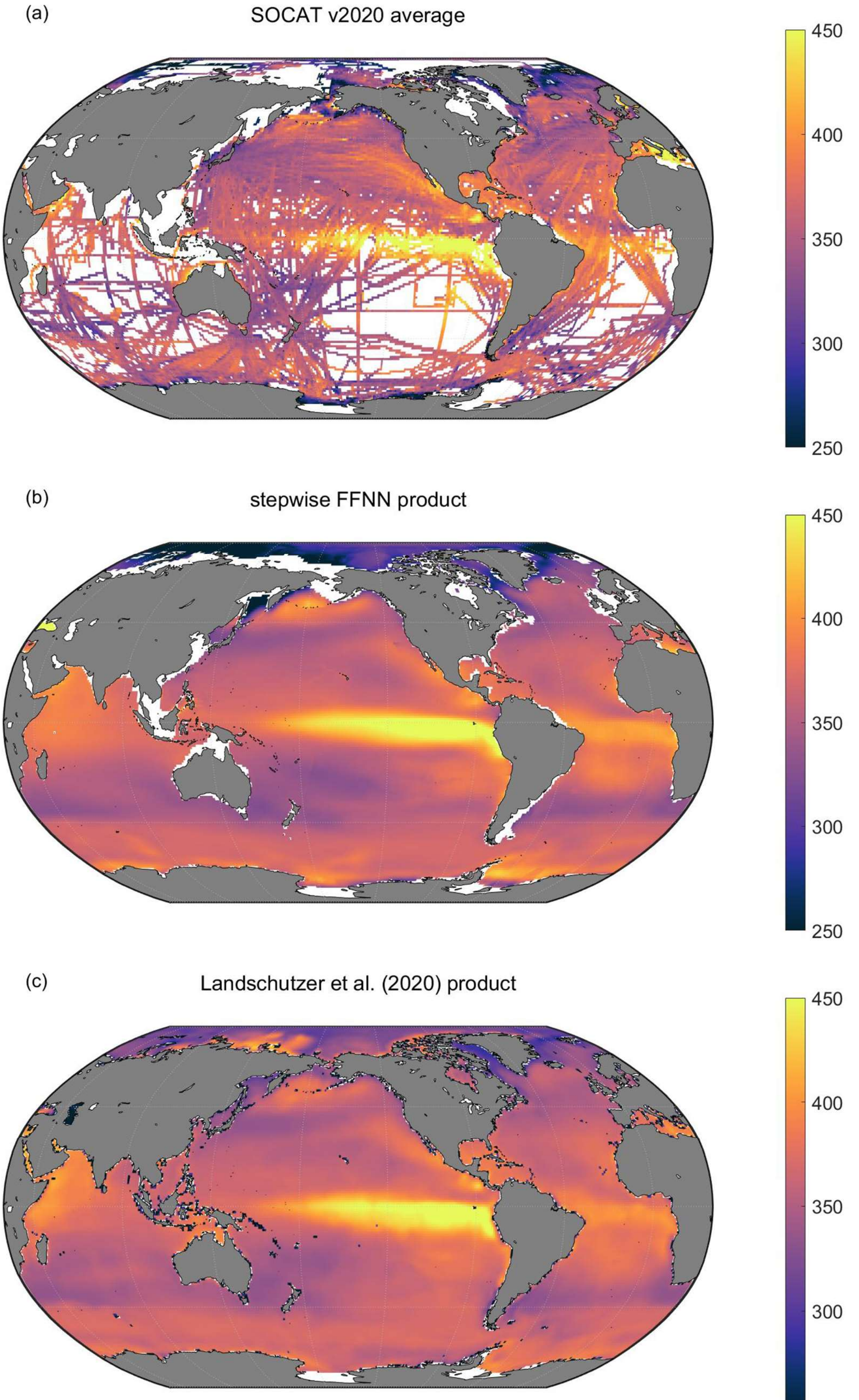

Figure 8. Comparison between long term average of a): SOCAT v2020 dataset, b): the stepwise

FFNN pCO_2 product and c): previous climatology product adapted from Landschützer et al., 2020.

4. Conclusions

A stepwise FFNN algorithm was constructed to decreasing the predicating error in the surface ocean pCO_2 mapping by finding better combinations of pCO_2 predictors in each biogeochemical province defined by SOM method, based on which a monthly 1°×1° gridded global open-oceanic surface ocean pCO_2 product from January 1992 to August 2019 was constructed. Our work provided a statistical way of predictor selection for all researches based on relationship fitting by machine learning methods, and shows that using regional-specific predictors selected by the stepwise FFNN algorithm retrieved lower predicting error than using globally same predictors. This stepwise FFNN algorithm can be also used in pCO_2 mapping researches for higher resolution and coastal regions, and also in other data mapping researches using SOM or other region dividing method. The prepare work was only collecting as many parameters, which are possibly related to the target data and need to be sufficiently available in time and space. However, high predicting error in special regions still remains to be improved, such as polar regions and equatorial Pacific. Since the result of the stepwise FFNN largely depends on the way biogeochemical provinces divided, improving of SOM step is still necessary. Besides, the FFNN can be replaced by any suitable type of neural networks. A possible way to improve the performance of stepwise FFNN algorithm is to modify the structure of FFNN or to use better networks. In the future work, the stepwise FFNN algorithm with possible improvement will be attempted in the mapping of other parameters, such as total alkalinity and pH, to provide more sufficient data support for studies on ocean acidification and carbon cycling.

Code and data availability

The stepwise FFNN algorithm (as a .m file for MATLAB) and the global 1°×1° gridded surface ocean pCO_2 product since from January 1992 to August 2019 (as a NetCDF file) generated during this study is available from the Institute of Oceanology of the Chinese Academy of Sciences Marine Science Data Center at http://dx.doi.org/10.12157/iocas.2021.0022 or directly at http://english.casodc.com/data/metadata-special-detail?id=1418424272359075841 .

Author contribution

Ma Jun, Yuan Huamao and Duan Liqin collected the dataset of pCO_2 predictors, and Qu baoxiao and Wang Yanjun was contributed in the synthesis of datasets. Zhong Guorong, Li Xuegang and Song Jinming designed the predictor selection algorithm and

performed the reconstruction of pCO_2 product. Wang Fan, Zhang Bin, Sun Xiaoxia, Zhang Wuchang, and Wang Zhenyan were contributed in the further improving. Zhong Guorong prepared the manuscript with contributions from all co-authors.

Competing interests

The authors declare that they have no conflict of interest.

Acknowledgement

This work was supported by The National Key Research and Development Program of China (No. 2017YFA0603204), the Strategic Priority Research Program of the Chinese Academy of Sciences (No. XDA19060401), National Natural Science Foundation of China (No. 91958103 and No. 42176200), and Natural Science Foundation of Shandong Province (ZR2020YQ28). We thank SOCAT for sharing the fCO_2 observation data. The Surface Ocean CO_2 Atlas (SOCAT) is an international effort, endorsed by the International Ocean Carbon Coordination Project (IOCCP), the Surface Ocean Lower Atmosphere Study (SOLAS) and the Integrated Marine Biosphere Research (IMBeR) program, to deliver a uniformly quality-controlled surface ocean CO_2 database. The many researchers and funding agencies responsible for the collection of data and quality control are thanked for their contributions to SOCAT. We thank NASA Goddard Space Flight Center, Ocean Ecology Laboratory, Ocean Biology Processing Group for sharing the Chlorophyll concentration data.

References

Bakker, D. C. E., Pfeil, B., Landa, C. S., Metzl, N., O'Brien, K. M., Olsen, A., Smith, K., Cosca, C., Harasawa, S., Jones, S. D., Nakaoka, S.-i., Nojiri, Y., Schuster, U., Steinhoff, T., Sweeney, C., Takahashi, T., Tilbrook, B., Wada, C., Wanninkhof, R., Alin, S. R., Balestrini, C. F., Barbero, L., Bates, N. R., Bianchi, A. A., Bonou, F., Boutin, J., Bozec, Y., Burger, E. F., Cai, W.-J., Castle, R. D., Chen, L., Chierici, M., Currie, K., Evans, W., Featherstone, C., Feely, R. A., Fransson, A., Goyet, C., Greenwood, N., Gregor, L., Hankin, S., Hardman-Mountford, N. J., Harlay, J., Hauck, J., Hoppema, M., Humphreys, M. P., Hunt, C., Huss, B., Ibanhez, J. S. P., Johannessen, T., Keeling, R., Kitidis, V., Koertzinger, A., Kozyr, A., Krasakopoulou, E., Kuwata, A., Landschützer, P., Lauvset, S. K., Lefevre, N., Lo Monaco, C., Manke, A., Mathis, J. T., Merlivat, L., Millero, F. J., Monteiro, P. M. S., Munro, D. R., Murata, A., Newberger, T., Omar, A. M., Ono, T., Paterson, K., Pearce, D., Pierrot, D., Robbins, L. L., Saito, S., Salisbury, J., Schlitzer, R., Schneider, B., Schweitzer, R., Sieger, R., Skjelvan, I., Sullivan, K. F., Sutherland, S. C., Sutton, A. J., Tadokoro, K., Telszewski, M., Tuma, M., van Heuven, S. M. A. C., Vandemark, D., Ward, B., Watson, A. J., and Xu, S.: A multi-decade record of high-quality fCO_2 data in version 3 of the Surface Ocean CO_2 Atlas (SOCAT), Earth System Science Data, 8, 383-413, 10.5194/essd-8-383-2016, 2016.

Bates, N. R.: Interannual variability of the oceanic CO_2 sink in the subtropical gyre of the North Atlantic Ocean over the last 2 decades, Journal of Geophysical Research: Oceans, 112, 2007.

Broullón, D., Pérez, F. F., Velo, A., Hoppema, M., Olsen, A., Takahashi, T., Key, R. M., Tanhua, T., González-Dávila, M., Jeansson, E., Kozyr, A., and van Heuven, S. M. A. C.: A global monthly climatology of total alkalinity: a neural network approach, Earth System Science Data, 11, 1109-1127, 10.5194/essd-11-1109-2019, 2019.

Broullon, D., Perez, F. F., Velo, A., Hoppema, M., Olsen, A., Takahashi, T., Key, R. M., Tanhua, T., Magdalena Santana-Casiano, J., and Kozyr, A.: A global monthly climatology of oceanic total dissolved inorganic carbon: a neural network approach, Earth System Science Data, 12, 1725-1743, 10.5194/essd-12-1725-2020, 2020.

Chen, L. Q., Xu, S. Q., Gao, Z. Y., Chen, H. Y., Zhang, Y. H., Zhan, J. Q., and Li, W.: Estimation of monthly air-sea CO_2 flux in the southern Atlantic and Indian Ocean using in-situ and remotely sensed data, Remote Sensing of Environment, 115, 1935-1941, 10.1016/j.rse.2011.03.016, 2011.

Cheng L. and J. Zhu: Benefits of CMIP5 multimodel ensemble in reconstructing historical ocean subsurface temperature variation, Journal of Climate, 29(15), 5393–5416, 10.1175/JCLI-D-15-0730.1, 2016.

Cheng L., K. Trenberth, J. Fasullo, T. Boyer, J. Abraham, J. Zhu: Improved estimates of ocean heat content from 1960 to 2015, Science Advances, 3, e1601545, 2017.

Cheng L., K. E. Trenberth, N. Gruber, J. P. Abraham, J. Fasullo, G. Li, M. E. Mann, X. Zhao, Jiang Zhu: Improved estimates of changes in upper ocean salinity and the hydrological cycle. Journal of Climate, 33, 10357–10381, 10.1175/JCLI-D-20-0366.1, 2020.

Chen, S., Hu, C., Barnes, B. B., Wanninkhof, R., Cai, W.-J., Barbero, L., and Pierrot, D.: A machine learning approach to estimate surface ocean pCO_2 from satellite measurements, Remote Sensing of Environment, 228, 203-226, 10.1016/j.rse.2019.04.019, 2019.

Chen, S. L., Hu, C. M., Byrne, R. H., Robbins, L. L., and Yang, B.: Remote estimation of surface pCO_2 on the West Florida Shelf, Continental Shelf Research, 128, 10-25, 10.1016/j.csr.2016.09.004, 2016.

Chen, S. L., Hu, C. M., Cai, W. J., and Yang, B.: Estimating surface pCO_2 in the northern Gulf of Mexico: Which remote sensing model to use?, Continental Shelf Research, 151, 94-110, 10.1016/j.csr.2017.10.013, 2017.

Commerce, U. D. o., Administration, N. O. a. A., and Center, N. G. D.: 2-minute Gridded Global Relief Data (ETOPO2v2). http://www.ngdc.noaa.gov/mgg/fliers/06mgg01.html, 2006.

Dee, D. P., Uppala, S. M., Simmons, A. J., Berrisford, P., Poli, P., Kobayashi, S., Andrae, U., Balmaseda, M. A., Balsamo, G., Bauer, P., Bechtold, P., Beljaars, A. C. M., van de Berg, L., Bidlot, J., Bormann, N., Delsol, C., Dragani, R., Fuentes, M., Geer, A. J., Haimberger, L., Healy, S. B., Hersbach, H., Holm, E. V., Isaksen, L., Kallberg, P., Kohler, M., Matricardi, M., McNally, A. P., Monge-Sanz, B. M., Morcrette, J. J., Park, B. K., Peubey, C., de Rosnay, P., Tavolato, C., Thepaut, J. N., and Vitart, F.: The ERA-Interim reanalysis: configuration and performance of the data assimilation system, Q J Roy Meteor Soc, 137, 553-597, 10.1002/qj.828, 2011.

Denvil-Sommer, A., Gehlen, M., Vrac, M., and Mejia, C.: LSCE-FFNN-v1: a two-step neural network model for the reconstruction of surface ocean pCO_2 over the global ocean, Geoscientific Model Development, 12, 2091-2105, 10.5194/gmd-12-2091-2019, 2019.

Dore, J. E., Lukas, R., Sadler, D. W., Church, M. J., and Karl, D. M.: Physical and biogeochemical modulation of ocean acidification in the central North Pacific, Proceedings of the National Academy of Sciences, 106, 12235-12240, 2009.

Friedlingstein, P., Jones, M. W., O'Sullivan, M., Andrew, R. M., Hauck, J., Peters, G. P., Peters, W., Pongratz, J., Sitch, S., Le Quere, C., Bakker, D. C. E., Canadell, J. G., Ciais, P., Jackson, R. B., Anthoni, P., Barbero, L., Bastos, A., Bastrikov, V., Becker, M., Bopp, L., Buitenhuis, E., Chandra, N., Chevallier, F., Chini, L. P., Currie, K. I., Feely, R. A., Gehlen, M., Gilfillan, D., Gkritzalis, T., Goll, D. S., Gruber, N., Gutekunst, S., Harris, I., Haverd, V., Houghton, R. A., Hurtt, G., Ilyina, T., Jain, A. K., Joetzjer, E., Kaplan, J. O., Kato, E., Goldewijk, K. K., Korsbakken, J. I., Landschützer, P., Lauvset, S. K., Lefevre, N., Lenton, A., Lienert, S., Lombardozzi, D., Marland, G., McGuire, P. C., Melton, J. R., Metzl, N., Munro, D. R., Nabel, J. E. M. S., Nakaoka, S.-I., Neill, C., Omar, A. M., Ono, T., Peregon, A., Pierrot, D., Poulter, B., Rehder, G., Resplandy, L., Robertson, E., Rodenbeck, C., Seferian, R., Schwinger, J., Smith, N., Tans, P. P., Tian, H., Tilbrook, B., Tubiello, F. N., van der Werf, G. R., Wiltshire, A. J., and Zaehle, S.: Global Carbon Budget 2019, Earth System Science Data, 11, 1783-1838, 10.5194/essd-11-1783-2019, 2019.

Friedrich, T., and Oschlies, A.: Neural network-based estimates of North Atlantic surface pCO_2 from satellite data: A methodological study, Journal of Geophysical Research-Oceans, 114, Artn C03020, 10.1029/2007jc004646, 2009.

Garcia, H., Weathers, K., Paver, C., Smolyar, I., Boyer, T., Locarnini, M., Zweng, M., Mishonov, A., Baranova, O., and Seidov, D.: World Ocean Atlas 2018. Vol. 4: Dissolved Inorganic Nutrients (phosphate, nitrate and nitrate+ nitrite, silicate), 2019a.

Garcia, H., Weathers, K., Paver, C., Smolyar, I., Boyer, T., Locarnini, M., Zweng, M., Mishonov, A., Baranova, O., and Seidov, D.: World Ocean Atlas 2018, Volume 3: Dissolved Oxygen, Apparent Oxygen Utilization, and Dissolved Oxygen Saturation, 2019b.

GLOBALVIEW-CO2: Cooperative Atmospheric Data Integration Project - Carbon Dioxide [CD-ROM]. NOAA ESRL, B., Colo. (Ed.), [Available at ftp.cmdl.noaa.gov, path: ccg/co2/GLOBALVIEW, 5th January 2013.], 2011.

González-Dávila, M., and Santana-Casiano, J.: Sea surface and atmospheric fCO_2 data measured during the estoc time series cruises from 1995-2009, CDIAC, Oak Ridge National Laboratory, US Department of Energy, Oak Ridge, Tennessee. doi, 10, 2009.

Gregor, L., Lebehot, A. D., Kok, S., & Scheel Monteiro, P. M. A comparative assessment of the uncertainties of global surface ocean CO_2 estimates using a machine-learning ensemble (CSIR-ML6 version 2019a)–have we hit the wall?. Geoscientific Model Development, 12(12), 5113-5136, 2019.

Hales, B., Strutton, P. G., Saraceno, M., Letelier, R., Takahashi, T., Feely, R., Sabine, C., and Chavez, F.: Satellite-based prediction of pCO_2 in coastal waters of the eastern North Pacific, Prog Oceanogr, 103, 1-15, 10.1016/j.pocean.2012.03.001, 2012.

Huang, B., Thorne, P. W., Banzon, V. F., Boyer, T., Chepurin, G., Lawrimore, J. H., Menne, M. J., Smith, T. M., Vose, R. S., and Zhang, H.-M.: Extended reconstructed sea surface temperature, version 5 (ERSSTv5): upgrades, validations, and intercomparisons, J Climate, 30, 8179-8205, 2017.

Iida, Y., Kojima, A., Takatani, Y., Nakano, T., Midorikawa, T., and Ishii, M.: Trends in $p$$CO_2$ and sea-air CO_2 flux over the global open oceans for the last two decades, J. Oceanogr., 71, 637–661, 10.1007/s10872-015-0306-4, 2015.

Jo, Y. H., Dai, M. H., Zhai, W. D., Yan, X. H., and Shang, S. L.: On the variations of sea surface $p$$CO_2$ in the northern South China Sea: A remote sensing based neural network approach, Journal of Geophysical Research-Oceans, 117, Artn C08022, 10.1029/2011jc007745, 2012.

Körtzinger, A.: Determination of carbon dioxide partial pressure ($p$$CO_2$), 3rd ed., Methods of Seawater Analysis, 3rd edn., 1999.

Landschützer, P., Gruber, N., Bakker, D. C. E., and Schuster, U.: Recent variability of the global ocean carbon sink, Glob. Biogeochem. Cycle, 28, 927-949, 10.1002/2014gb004853, 2014.

Landschützer, P., Gruber, N., Bakker, D. C. E., Schuster, U., Nakaoka, S., Payne, M. R., Sasse, T. P., and Zeng, J.: A neural network-based estimate of the seasonal to inter-annual variability of the Atlantic Ocean carbon sink, Biogeosciences, 10, 7793-7815, 10.5194/bg-10-7793-2013, 2013.

Landschützer, P., Gruber, N., and Bakker, D. C. E.: Decadal variations and trends of the global ocean carbon sink, Glob. Biogeochem. Cycle, 30, 1396-1417, 10.1002/2015gb005359, 2016.

Landschützer, P., Laruelle, G. G., Roobaert, A., and Regnier, P.: A uniform $p$$CO_2$ climatology combining open and coastal oceans, Earth Syst. Sci. Data Discuss., 2020, 1-30, 10.5194/essd-2020-90, 2020.

Laruelle, G. G., Landschützer, P., Gruber, N., Tison, J. L., Delille, B., and Regnier, P.: Global high-resolution monthly $p$$CO_2$ climatology for the coastal ocean derived from neural network interpolation, Biogeosciences, 14, 4545-4561, 10.5194/bg-14-4545-2017, 2017.

Marrec, P., Cariou, T., Mace, E., Morin, P., Salt, L. A., Vernet, M., Taylor, B., Paxman, K., and Bozec, Y.: Dynamics of air-sea CO_2 fluxes in the northwestern European shelf based on voluntary observing ship and satellite observations, Biogeosciences, 12, 5371-5391, 10.5194/bg-12-5371-2015, 2015.

Marshall G J.: Trends in the Southern Annular Mode from observations and reanalyses, Journal of climate, 16, 10.1175/1520-0442(2003)016<4134:TITSAM>2.0.CO;2, 4134-4143, 2003.

Menemenlis, D., Campin, J.-M., Heimbach, P., Hill, C., Lee, T., Nguyen, A., Schodlok, M., and Zhang, H.: ECCO2: High Resolution Global Ocean and Sea Ice Data Synthesis, Mercator Ocean Quarterly Newsletter, 2008.

Moussa, H., Benallal, M. A., Goyet, C., and Lefevre, N.: Satellite-derived CO_2 fugacity in surface seawater of the tropical Atlantic Ocean using a feedforward neural network, Int J Remote Sens, 37, 580-598, 10.1080/01431161.2015.1131872, 2016.

Nakaoka, S., Telszewski, M., Nojiri, Y., Yasunaka, S., Miyazaki, C., Mukai, H., and Usui, N.: Estimating temporal and spatial variation of ocean surface $p$$CO_2$ in the

North Pacific using a self-organizing map neural network technique, Biogeosciences, 10, 6093-6106, 10.5194/bg-10-6093-2013, 2013.

NASA Goddard Space Flight Center, Ocean Ecology Laboratory, Ocean Biology Processing Group. Moderate-resolution Imaging Spectroradiometer (MODIS) Aqua Chlorophyll Data; 2018 Reprocessing. NASA OB.DAAC, Greenbelt, MD, USA. 10.5067/AQUA/MODIS/L3M/CHL/2018, 2018.

Rödenbeck, C., Bakker, D. C. E., Metzl, N., Olsen, A., Sabine, C., Cassar, N., Reum, F., Keeling, R. F., and Heimann, M.: Interannual sea–air CO_2 flux variability from an observationdriven ocean mixed-layer scheme, Biogeosciences, 11, 4599–4613, 10.5194/bg-11-4599-2014, 2014.

Sabine, C. L., Feely, R. A., Gruber, N., Key, R. M., Lee, K., Bullister, J. L., Wanninkhof, R., Wong, C. S., Wallace, D. W. R., Tilbrook, B., Millero, F. J., Peng, T. H., Kozyr, A., Ono, T., and Rios, A. F.: The oceanic sink for anthropogenic CO_2, Science, 305, 367-371, DOI 10.1126/science.1097403, 2004.

Sarma, V. V. S. S., Saino, T., Sasaoka, K., Nojiri, Y., Ono, T., Ishii, M., Inoue, H. Y., and Matsumoto, K.: Basin-scale pCO_2 distribution using satellite sea surface temperature, Chl-a, and climatological salinity in the North Pacific in spring and summer, Glob. Biogeochem. Cycle, 20, Artn Gb3005, 10.1029/2005gb002594, 2006.

Shadwick, E. H., Thomas, H., Comeau, A., Craig, S. E., Hunt, C. W., and Salisbury, J. E.: Air-Sea CO_2 fluxes on the Scotian Shelf: seasonal to multi-annual variability, Biogeosciences, 7, 3851-3867, 10.5194/bg-7-3851-2010, 2010.

Signorini, S. R., Mannino, A., Najjar, R. G., Friedrichs, M. A. M., Cai, W. J., Salisbury, J., Wang, Z. A., Thomas, H., and Shadwick, E.: Surface ocean pCO_2 seasonality and sea-air CO_2 flux estimates for the North American east coast, Journal of Geophysical Research-Oceans, 118, 5439-5460, 10.1002/jgrc.20369, 2013.

Takahashi, T., Sutherland, S. C., Feely, R. A., and Wanninkhof, R.: Decadal change of the surface water pCO_2 in the North Pacific: A synthesis of 35 years of observations, Journal of Geophysical Research-Oceans, 111, Artn C07s05, 10.1029/2005jc003074, 2006.

Takahashi, T., Sutherland, S. C., Wanninkhof, R., Sweeney, C., Feely, R. A., Chipman, D. W., Hales, B., Friederich, G., Chavez, F., Sabine, C., Watson, A., Bakker, D. C. E., Schuster, U., Metzl, N., Yoshikawa-Inoue, H., Ishii, M., Midorikawa, T., Nojiri, Y., Kortzinger, A., Steinhoff, T., Hoppema, M., Olafsson, J., Arnarson, T. S., Tilbrook, B., Johannessen, T., Olsen, A., Bellerby, R., Wong, C. S., Delille, B., Bates, N. R., and de Baar, H. J. W.: Climatological mean and decadal change in surface ocean pCO_2, and net sea-air CO_2 flux over the global oceans, Deep-Sea Research Part Ii-Topical Studies in Oceanography, 56, 554-577, 10.1016/j.dsr2.2008.12.009, 2009.

Telszewski, M., Chazottes, A., Schuster, U., Watson, A. J., Moulin, C., Bakker, D. C. E., Gonzalez-Davila, M., Johannessen, T., Kortzinger, A., Luger, H., Olsen, A., Omar, A., Padin, X. A., Rios, A. F., Steinhoff, T., Santana-Casiano, M., Wallace, D. W. R., and Wanninkhof, R.: Estimating the monthly pCO_2 distribution in the North Atlantic using a self-organizing neural network, Biogeosciences, 6, 1405-1421, DOI 10.5194/bg-6-1405-2009, 2009.

Wang, Y., Li, X., Song, J., Zhong, G., and Zhang, B.: Carbon Sinks and Variations of *p*CO_2 in the Southern Ocean from 1998 to 2018 Based on a Deep Learning Approach, IEEE Journal of Selected Topics in Applied Earth Observations and Remote Sensing, 2021.

Watson, A. J., Schuster, U., Shutler, J. D., Holding, T., Ashton, I. G. C., Landschützer, P., Woolf, D. K., and Goddijn-Murphy, L.: Revised estimates of ocean-atmosphere CO_2 flux are consistent with ocean carbon inventory, Nature Communications, 11, 10.1038/s41467-020-18203-3, 2020.

Weiss, R. F.: Carbon dioxide in water and seawater: the solubility of a non-ideal gas, Marine Chemistry, 2, 203--215, 1974.

Zeng, J., Nojiri, Y., Landschützer, P., Telszewski, M., and Nakaoka, S.: A Global Surface Ocean *f*CO_2 Climatology Based on a Feed-Forward Neural Network, Journal of Atmospheric and Oceanic Technology, 31, 1838-1849, 10.1175/jtech-d-13-00137.1, 2014.

Zeng, J. Y., Nojiri, Y., Nakaoka, S., Nakajima, H., and Shirai, T.: Surface ocean CO_2 in 1990-2011 modelled using a feed-forward neural network, Geosci Data J, 2, 47-51, 10.1002/gdj3.26, 2015.

Zeng, J. Y., Matsunaga, T., Saigusa, N., Shirai, T., Nakaoka, S., and Tan, Z. H.: Technical note: Evaluation of three machine learning models for surface ocean CO_2 mapping, Ocean Sci, 13, 303-313, 10.5194/os-13-303-2017, 2017.

Zhong, G., Li, X., Qu, B., Wang, Y., Yuan, H, and Song, J.: A General Regression Neural Network approach to reconstruct global 1°×1° resolution sea surface *p*CO_2, Acta Oceanol Sin, 10, 70-79, 10.3969/j.issn.0253-4193.2020.10.007, 2020.